Encapsulation of epitaxial silicene on ZrB$_2$ with NaCl

F. B. Wiggers, , Y. Yamada-Takamura, , A. Y. Kovalgin, and , and M. P. de Jong

Encapsulation of epitaxial silicene on ZrB$_2$ with NaCl

F. B. Wiggers,[1,a)] Y. Yamada-Takamura,[2] A. Y. Kovalgin,[1] and M. P. de Jong[1]

[1]*MESA+ Institute for Nanotechnology, University of Twente, 7500 AE Enschede, The Netherlands*
[2]*School of Materials Science, Japan Advanced Institute of Science and Technology, Nomi, Ishikawa 923-1292, Japan*

Silicene and other two-dimensional materials, such as germanene and stanene, have chemically reactive surfaces and are prone to oxidation in air, and thus require an encapsulation layer for *ex situ* studies or integration in an electronic device. In this work, we investigated NaCl as an encapsulation material for silicene. NaCl was deposited on the surface of epitaxial silicene on ZrB$_2$(0001) thin films near room temperature and studied using synchrotron-based high-resolution photoelectron spectroscopy. The deposition of NaCl resulted in dissociative chemisorption, where the majority of epitaxial silicene reacted to form Si–Cl$_x$ species. *Published by AIP Publishing.* [http://dx.doi.org/10.1063/1.4985895]

INTRODUCTION

Silicene is a two-dimensional (2D) material with a honeycomb lattice of Si atoms.[1] As a Dirac material, it is predicted to exhibit unique properties, such as the quantum spin Hall effect[2] corresponding to a 2D topological insulator phase, with applications in spintronics. Epitaxial silicene layers have been synthesized in ultra-high vacuum on a number of substrates, such as Ag(111),[3] Ir(111),[4] and ZrB$_2$(0001),[5] and have been characterized using surface science techniques. Unlike graphene, silicene is chemically reactive and can react with, e.g., oxygen and water in the air, significantly altering its electronic properties. While this property can be favorably exploited for chemical modification, it hampers *ex situ* characterization and integration in an electronic device. This can be solved by encapsulation of the single-atom-thick layer. The encapsulation layer then functions as both a protective layer and a gate dielectric layer, enabling characterization and integration. The recent synthesis of quasi-freestanding silicene on oxidized silicon,[6] thereby electrically isolating it from its substrate, emphasizes the need for the development of a compatible encapsulation layer. In addition, ultra-thin films and other two-dimensional materials, such as germanene and stanene, that are also chemically reactive would also benefit from an encapsulation layer that preserves the structural and electronic properties of the layer underneath.

Since silicene is chemically reactive, encapsulating it without altering either its lattice or electronic structure poses a serious challenge. To date, there are only two reported methods for encapsulation of silicene with a dielectric material. The first method requires the growth of multilayer silicene, where a thin native Si oxide layer in the surface region of the film that is exposed to air preserves the integrity of the rest of the silicene.[7] The second method involves the encapsulation of silicene with Al$_2$O$_3$.[8] This was accomplished by

depositing Al with an oxygen pressure of 10^{-6} mbar. However, such a process requires careful tailoring to prevent an excess of elemental Al or oxidation of the silicene layer. The latter difficulty was observed in our previous work with the deposition and subsequent oxidation of a sub-monolayer of Al on silicene on ZrB$_2$(0001) with O$_2$.[9] It was found that the Al atoms catalyze the chemical dissociation of the O$_2$ molecules into oxygen atoms that then also react with silicene.

An encapsulation layer that involves a simpler and more robust deposition method would therefore be of great advantage. In this regard, alkali metal halides offer an attractive solution since they are electrically insulating and do not contain oxygen or carbon atoms. We investigated the deposition of NaCl on epitaxial silicene. There are drawbacks to using NaCl as an encapsulation layer: (i) the strongly varying surface potential associated with the ionic bonds could affect the electronic properties of the silicene layer, and (ii) it may absorb water from air leading to degradation of the encapsulation layer. However, it has been reported previously that NaCl was successfully used to encapsulate and protect a surface from oxidation.[10] In addition, long-term stability can be ensured by depositing an additional layer that functions specifically as a barrier to water and air, e.g., Al$_2$O$_3$. The advantages of using NaCl as an encapsulation material are clear as it involves a single-step evaporation process and provides an electrically insulating and optically transparent layer, owing to its 8.5 eV bandgap.[11] In addition, NaCl does not exhibit first-order Raman scattering,[12] minimizing interference with *ex situ* measurements of silicene by Raman spectroscopy.

In this work, we studied the deposition of NaCl on the surface of epitaxial silicene on ZrB$_2$(0001) thin films using synchrotron-based high-resolution photoelectron spectroscopy (HR-PES). Core-level binding energies are very sensitive to the chemical environment and the bonding configuration in the vicinity of the atoms where the excitation occurs. Using this powerful spectroscopic technique, we provide

---

a)Author to whom correspondence should be addressed: F.B.Wiggers@utwente.nl

information on the chemical interaction between NaCl and epitaxial silicene.

EXPERIMENTAL

Single-crystalline ZrB_2 epitaxial thin films were grown on Si(111) substrates by ultra-high vacuum chemical vapor epitaxy, which is described elsewhere.[13] All subsequent sample preparation steps and measurements were performed at the MatLine beamline of the ASTRID2 synchrotron at the University of Aarhus, Denmark. The endstation consists of a loadlock (base pressure 1×10^{-7} mbar) and an analysis chamber (base pressure 4×10^{-10} mbar) equipped with a Scienta SES200 hemispherical analyzer for HR-PES measurements. Annealing is carried out in the analysis chamber by means of e-beam heating, while the temperature is measured using a thermocouple and a pyrometer. The same chamber is also equipped with a LEED system. The loadlock is equipped with the NaCl deposition source.

Sample preparation involves annealing at 800 °C in ultra-high vacuum, which is known to terminate the surface with a monolayer of silicene, with Si originating from the Si substrate.[5] Following sample preparation, the samples were investigated *in situ* by LEED and HR-PES. All HR-PES measurements were carried out with the sample normal directed towards the photoelectron analyzer and with the photon source at a 45° angle to the surface normal.

The Si 2p spectra were measured using a photon energy of 150 eV. The binding energy scale of the Si 2p spectrum of the as-annealed surface is calibrated using the dominant Si $2p_{3/2}$ peak at 98.98 eV of pristine silicene on ZrB_2.[14] The possible errors in binding energy in the subsequent spectra caused by varying conditions of the beamline and storage ring are corrected for by measuring the Si 2p spectrum immediately before and after any sample treatment. The binding energy scale of the B 1s and Zr 3d spectrum of the pristine surface, measured using a photon energy of 240 eV, has been calibrated using 181.4 eV and 179.0 eV for the Zr $3d_{3/2}$ and Zr $3d_{5/2}$ peaks, respectively, corresponding to Zr atoms in a silicene-terminated $ZrB_2(0001)$ thin film. The same correction value has also been applied to all subsequent spectra. The Na 2p and Cl 2p spectra were measured using a photon energy of 80 eV and 250 eV, respectively. The Na 2p and Cl 2p binding energy scales are calibrated using the errors found by linear extrapolation using the errors in the binding energy scales of the Si 2p and Zr 3d spectra. All spectra are normalized to the beam current in the storage ring.

The NaCl deposition source consists of a glass lightbulb enclosed by a Ta shroud, to which a thermocouple is attached, except for an opening at the top, and operates by thermal evaporation of NaCl powder (≥99.5% purity, Sigma Aldrich) contained within. NaCl deposition was carried out by exposing the sample surface, held within the line-of-sight of the source opening and filament at a distance of approximately 10 cm, at room temperature to the NaCl flux at a background pressure of 2×10^{-7} mbar. We note that the actual sample temperature was slightly higher than room temperature due to radiative heating from the source. Previous mass spectrometry studies have shown that NaCl vaporizes as NaCl (monomer) and

Na_2Cl_2 (dimer) molecules. The monomers (majority species) and the dimers (minority species) have partial pressures of the same order of magnitude.[15] The amount of NaCl deposited is estimated based on the suppression of core levels.

RESULTS AND DISCUSSION

After introducing the sample into the ultra-high vacuum system, it was annealed at 800 °C to remove the native oxide and prepare a pristine surface of silicene-terminated ZrB_2. This is confirmed by the Si 2p spectrum, shown in Fig. 1(a)(spectrum 1), that features the characteristic spectral envelope corresponding to silicene-terminated ZrB_2, as reported previously,[5] and is further supported by peak-fitting results, as discussed later. The Zr 3d and B 1s spectrum shown in Fig. 1(b) (spectrum 1) features a Zr 3d doublet, with the $3d_{3/2}$ and $3d_{5/2}$ peaks at 181.4 eV and 179.0 eV, and a B 1s peak, at 188.1 eV, corresponding to Zr and B atoms in the ZrB_2 thin film. In addition, LEED measurements (data not shown) feature the $ZrB_2(0001)$-(2×2) pattern, which is equivalent to the $(\sqrt{3} \times \sqrt{3})$-reconstruction pattern of silicene.

NaCl was deposited step-wise by five repetitions of deposition and HR-PES measurements, with the sample always at room temperature. The first four depositions were performed with an identical deposition time of 5 min and with identical NaCl source settings. The fifth and last deposition of NaCl also consisted of 5 min deposition time but with a higher NaCl source temperature.

The deposition of NaCl is confirmed by the appearance of Na 2p and Cl 2p peaks, as can be seen in Figs. 1(c) and 1(d) (spectra 1-2). Each deposition results in a continued increase in intensity for the Na 2p and Cl 2p peaks, as shown in Figs. 1(c) and 1(d) (spectra 3-6). The distance in binding energy of 1.6 eV between the two resolved peaks in the Cl 2p spectra corresponds to the spin-orbit splitting of the Cl 2p doublet.[16] The two weak peaks visible in the Na 2p spectrum in Fig. 1(c) (spectrum 1), centered at 27.6 eV and 29.1 eV binding energy, correspond to the Zr 4p doublet.

As a result of the deposition of NaCl on top of the silicene-terminated ZrB_2, the intensities of the Si 2p, Zr 3d, and B 1s peaks decrease, as shown in Figs. 1(a) and 1(b) (spectra 1-6). It is noted that with each of the first four depositions, the distance in binding energy between the B 1s and Zr 3d peaks decreases, causing a total shift of 50 meV. This can be explained by the outer Zr atoms that terminate the ZrB_2 thin film,[5,17] which are affected by the deposition and/or dissociative chemisorption of NaCl, which will be discussed later, resulting in an increase of the binding energy of the surface-related Zr 3d peak.

The integrated intensities of the core levels are shown in Fig. 2, normalized to their maximum areal intensity. The decrease in intensities of the Si 2p, Zr 3d, and B 1s core levels correlates well with the increase in Na 2p and Cl 2p intensities. The normalized intensities of the Na 2p and Cl 2p peaks are observed to increase linearly with the same rate for the first four depositions. This indicates that the stoichiometry of the deposited NaCl remains constant. The amount of NaCl deposited is estimated based on the suppression of the Si 2p, Zr 3d, and B 1s core levels. After the first four depositions, their intensities decrease to 31%-36%, corresponding to an effective
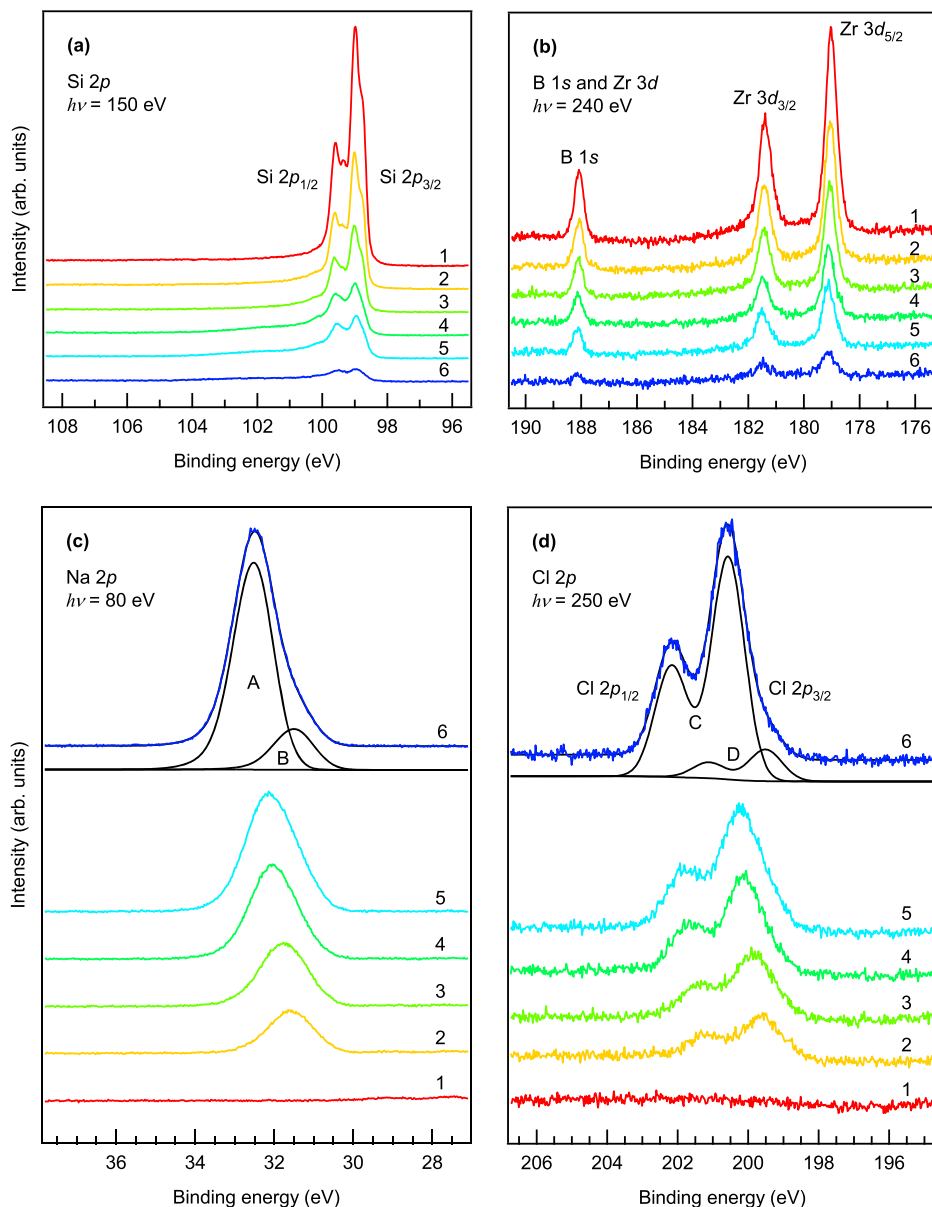
FIG. 1. High-resolution photoelectron spectra of (a) Si 2*p*, (b) B 1*s* and Zr 3*d*, (c) Na 2*p*, and (d) Cl 2*p* core-level regions detailing the results of NaCl deposition on the silicene-terminated ZrB$_2$ surface. The spectra are presented in chronological order: (1) pristine silicene, (2-5) deposition of 0.6 nm NaCl in four equal steps, and (6) deposition of a total of 1.2 nm NaCl. Peak-fitting results are shown for spectrum 6 of Na 2*p* and Cl 2*p*. The sum of the fitted data is plotted behind the measured data, while the two components and the background are offset.

NaCl layer thickness equal to 1 inelastic mean free path λ of the photoelectron,[18] i.e., 0.6 nm, according to an overlayer-substrate model. This corresponds to an average deposition
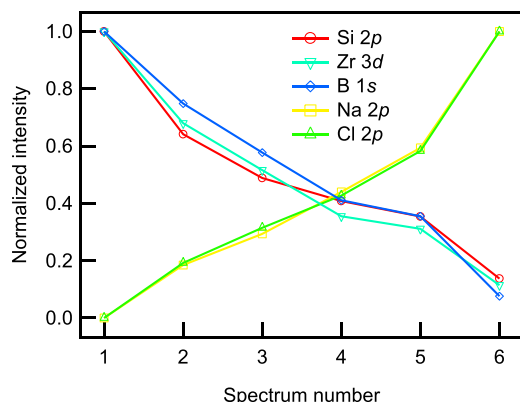

FIG. 2. The normalized integrated intensities of the core levels are compared. The spectrum number corresponds to the identification given in Figs. 1(a)–1(d).

rate of 0.03 nm/min. The larger increase and decrease for, respectively, Na 2*p* and Cl 2*p*, and Si 2*p*, Zr 3*d*, and B 1*s*, after the last deposition, are consistent with the increase in temperature of the NaCl source. After the final deposition, the intensities of the Si 2*p*, Zr 3*d*, and B 1*s* peaks decrease to 8%-14% corresponding to an effective NaCl thickness of 2 λ, i.e., 1.2 nm. This corresponds to a deposition rate of 0.12 nm/min for the final deposition. The growth mode of NaCl on silicene at room temperature is however not known and could also involve 3D island growth. Therefore, the results from the overlayer-substrate model should be regarded as a lower limit for the amount of NaCl that was deposited. Further, the suppression of 86% of the Si 2*p* core level after the final deposition step indicates that at least 86% of the Si is covered with NaCl.

THE Si 2*p* CORE LEVEL

The Si atoms in the silicene lattice on ZrB$_2$ occupy three distinct sites such that each contributes a Si 2*p* doublet to the

Si 2p spectrum.[19] The intensity ratio of Si 2$p_{1/2}$ to Si 2$p_{3/2}$ in each doublet is 1:2. The ratio of the 2$p_{1/2}$ and 2$p_{3/2}$ features in the Si 2p spectrum appears to decrease with each deposition step, as can be seen in Fig. 1(a) (spectra 1-6). This trend coincides with the appearance and subsequent increase in relative intensity of a component at 100.2 eV binding energy, forming a shoulder on the silicene spectrum. With the third deposition of NaCl, a weak, broad component appears at 102.0 eV, as shown in Fig. 1(a) (spectrum 4). These two new components are more easily observed in Fig. 3.

In order to better understand the changes in the Si 2p spectra, the spectra were peak fitted by least-squares fitting using a Shirley background and symmetric Gaussian line shapes, with each component consisting of a doublet with an area ratio of 1:2 for the Si 2$p_{1/2}$ and Si 2$p_{3/2}$ peaks and 0.6 eV spin-orbit splitting. The silicene-related peaks are based on a model of the silicene honeycomb lattice that consists of three unique sites occupied by Si atoms on the Zr-terminated ZrB$_2$ thin film.[5,19] These atomic sites give rise to peaks α, β, and γ in core-level PES[19] and were fitted with an area ratio of 2:3:1. The distance in binding energy of 230 meV between α and β, and 160 meV between β and γ, is the result of fitting using initial binding

energies based on previously reported fitting parameters.[19] The full-width-at-half-maximum (FWHM) was constrained to be equal among the three components of silicene in the spectrum of the as-annealed sample, and was fitted as 240 meV, and was fixed for subsequent spectra. For a more detailed discussion of the fitting parameters for epitaxial silicene on ZrB$_2$(0001), see the work of Lee *et al.*[19]

Figure 3 (spectrum 1) shows the peak-fitting results for the as-annealed sample, with 76% of the intensity attributed to silicene. The remaining intensity, in the broad component, can be explained by disordered Si or remaining Si sub-oxide after annealing. After NaCl deposition, the silicene-related peaks alone cannot be used to explain the spectral envelope, requiring a minimum of two additional peaks. These additional peaks, Si$_A$ and Si$_B$, are on average centered at 101.1 eV and 99.4 eV, respectively. The combination of these components is able to account for the complete spectral envelope through all spectra, as can been seen in Fig. 3.

The progression of the intensity of the Si$_A$, Si$_B$, and silicene-related components, normalized to the total Si 2p intensity, is shown in Fig. 4. Initially, silicene accounts for 76% of the total intensity, and the remaining intensity is represented by the broad feature Si$_B$. Note that the same feature Si$_B$ is used to represent Si species formed after NaCl deposition, as it is difficult to separate the contributions at similar binding energies, as shown in the spectra that follow. With increasing number of NaCl depositions, the relative intensity of silicene is observed to decrease. During the first few depositions, the increase in relative intensity of Si$_B$ is the easiest to notice. This explains the shoulder that is observed to form in the experimental data and also the apparent change in the Si 2$p_{1/2}$ to Si 2$p_{3/2}$ intensity ratio of silicene. After the third deposition (spectrum 4), the Si$_A$ component has increased noticeably and accounts for a significant portion of the total Si intensity. After the final deposition, 22% of the total Si intensity is attributed to silicene, suggesting that the majority of the silicene has reacted, as discussed below. The intensity attributed to remaining "silicene" can also be explained by Si atoms, formerly part of the silicene lattice, that did not react. The other 78% of the Si intensity resides in the two components Si$_A$ and Si$_B$, which are very broad peaks with 2.7 eV and 1.2 eV FWHM, respectively. It is therefore likely that these two components actually consist of multiple, unresolved components. As a consequence, assigning Si$_A$ and Si$_B$ to specific chemical species is not meaningful. Instead, in the following, we discuss two explanations that
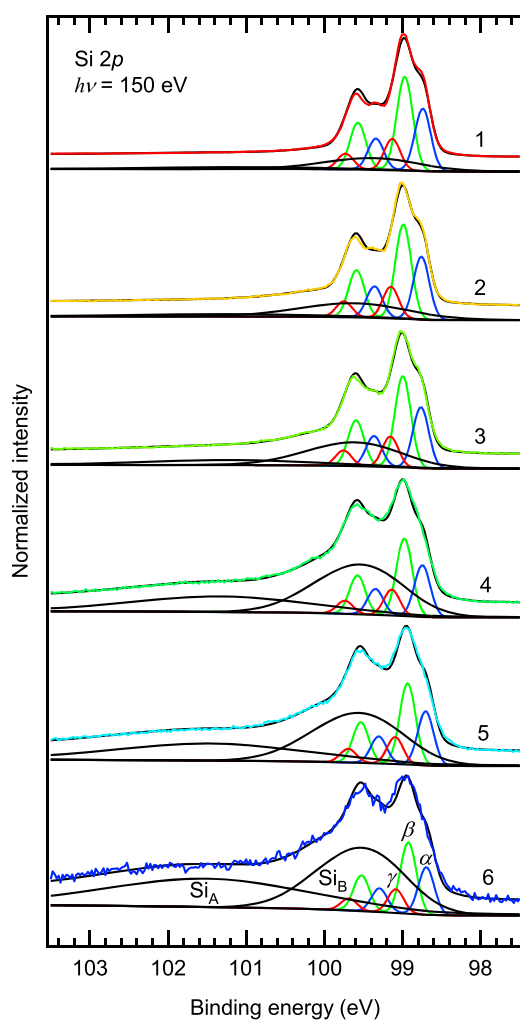

FIG. 3. The Si 2p spectra of Fig. 1(a) are normalized with respect to their maximum intensity and shown together with peak-fitting results. The sum of the fitted data is plotted behind the measured data, while the individual components and the background are offset.
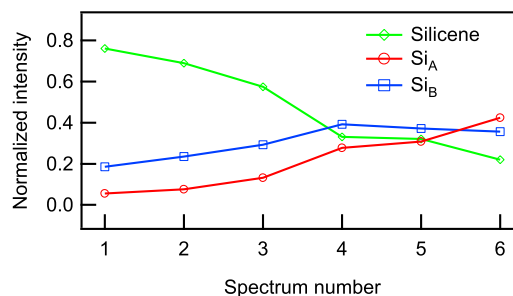

FIG. 4. The intensities of the fitted Si 2p components for each NaCl deposition step are shown, normalized with respect to the total Si intensity. The spectrum number corresponds to the identification given in Fig. 3.

involve chemical species with a chemical shift that places their Si $2p$ core level in the same binding energy range as covered by Si_A and Si_B.

One possible explanation is the dissociative chemisorption of NaCl, resulting in the formation of metallic Na, and Si–Cl_x species. This was previously observed by Chung *et al.* upon deposition of NaCl on Si(100), with a chemical shift of +0.9 eV for Si–Cl species relative to the bulk Si $2p_{3/2}$ peak.[20,21] Matsuo *et al.* studied the surface reaction of molecular and atomic chlorine on Si(100) and Si(111) and found not only Si–Cl by exposure to molecular chlorine but also Si–Cl_x (x = 2-4) by exposure to atomic chlorine.[22] They reported Si–Cl at a binding energy of 100.5 eV and an additional chemical shift of +1 eV for every additional chlorine bond. Rivillon *et al.* reported a shift of +0.83 eV and +1.37 eV for Si–Cl and Si–Cl_2, respectively, relative to the bulk Si $2p_{3/2}$ peak on chlorine-terminated Si(111).[23] In the current work, based on the reported chemical shifts, the Si_A and Si_B components overlap well with the expected binding energies of the Si–Cl_x (x = 1-3) species.

However, similar chemical shifts can also be caused by Si oxidation, which is possible as NaCl deposition took place with a background pressure of 10^{-7} mbar in a baked-out loadlock. Lu *et al.* reported on the chemical shift of Si oxidation states: +0.97 eV, +1.80 eV, +2.60 eV, and +3.82 eV shift, with respect to the Si bulk peak, for Si^{+1}, Si^{+2}, Si^{+3}, and Si^{+4}, respectively.[24] However, in a previous report, we showed that only a minor amount of Si sub-oxide is formed after exposing silicene on ZrB_2 to a dose of 4500 L of O_2 molecules, resulting in a Si $2p$ peak at 100.2 eV.[9] In the current work, the sample surface was exposed to a dose of 900 L while present in the loadlock, suggesting that Si (sub-)oxide formation is insignificant, assuming the background pressure was due to O_2 molecules. It is noted that although no O $1s$ peak was observed (data not shown), the sensitivity for the O $1s$ signal is low compared with Si $2p$, resulting in a limit of detection corresponding to 0.4 ML of O atoms.

Given the large Si $2p$ chemical shift associated with Si bonding with Cl, the large intensity closer in binding energy to that of the silicene-related peaks, well represented by component Si_B, could be explained by Si atoms affected by the formation of nearby Si–Cl species.

In summary, a majority of the silicene was affected after NaCl deposition, but from peak fitting, it followed that a small amount of intensity remained at the binding energies associated with silicene. The total Si $2p$ intensity decreased by 86%, suggesting that at least 86% of the Si was covered by NaCl.

THE Na $2p$ AND Cl $2p$ CORE LEVELS

After NaCl deposition, the Na $2p$ and Cl $2p$ spectra feature a doublet, as shown in Figs. 1(c) and 1(d) (spectrum 2). In addition, peak fitting performed on the final Na $2p$ and Cl $2p$ spectra, shown in Figs. 1(c) and 1(d) (spectrum 6), shows that a single doublet cannot explain the spectral line shapes and provides evidence for a second doublet for each core level, labelled B and D, respectively. It is assumed that the binding energy of 199.51 eV of the D component, corresponding to

the Cl $2p_{3/2}$ peak, remains the same between deposition steps, while component C shifts. Note that it is then increasingly difficult to peak fit the previous Cl $2p$ spectra 2-5, as the C component appears to shift closer in binding energy. The same explanation applies to B, at 31.44 eV binding energy, and A in the Na $2p$ spectrum.

The Cl $2p$ spectrum was peak fitted by least-squares fitting using a Shirley background and symmetric Gaussian line shapes, with each component consisting of a doublet with an area ratio of 1:2 for the Cl $2p_{1/2}$ and Cl $2p_{3/2}$ peaks and 1.60 eV spin-orbit splitting. The Na $2p$ spectrum was also peak fitted by least-squares fitting using a Shirley background, but used asymmetric Gaussian line shapes, with each component consisting of a doublet with an area ratio of 1:2 for the Na $2p_{1/2}$ and Na $2p_{3/2}$ peaks and 0.16 eV spin-orbit splitting.

The C and D components of Cl $2p$ in Fig. 1(d) (spectrum 6) are separated by 1.06 eV binding energy and their area ratio is 7.0. The A and B components of Na $2p$ in Fig. 1(c) (spectrum 6) are separated by 1.02 eV binding energy and their area ratio is 5.1. The distances in binding energy and the area ratios are similar and suggest that the A and B components of Na $2p$ correspond to the C and D components of Cl $2p$, respectively. The Na $2p$ and Cl $2p$ spectra can then be interpreted according to the explanation discussed previously for the Si $2p$ spectrum: dissociative chemisorption of NaCl and the formation of Si–Cl_x species. Based on spectrum 6, the A and C components are attributed to NaCl, given their greater intensity and taking into account the large amount of NaCl that was deposited, suppressing the components related to the dissociated species on the interface below. Accordingly, the B and D components are attributed to Na^+ and Si–Cl_x species, respectively.

The gradual increase in binding energies of the A and C components can be explained by two effects: (i) electrostatic charging and (ii) decreased screening of core holes by the metallic silicene/ZrB_2 substrate or a combination of both. Due to these effects, the Na and Cl atoms residing at different depths in the NaCl layer have different binding energies such that the A and C components actually consist of multiple, unresolved doublets.

Chang *et al.* also observed a shift in the peaks associated with NaCl, upon formation of NaCl by Na deposition on a Cl-terminated Si(100) surface.[21] They suggested that the shift was likely the result of the formation of a dipole-layer at the interface due to excess charge transfer from the Na adsorbates to the Si substrate.

The cumulative shift in binding energy of the Na $2p$ and Cl $2p$ core levels as a function of the NaCl layer thickness is shown in Fig. 5. The core-level shifts were evaluated from the binding energy position of maximum intensity. The Na $2p$ and Cl $2p$ core levels shift to higher binding energies by 0.91 eV and 1.00 eV in total, respectively. The increase in binding energy of both core levels between deposition steps is similar, except between spectra 2 and 3.

Ultra-thin layers of NaCl are reported to be unstable under electron irradiation as occurs when using LEED.[25] For this reason, LEED was performed only after the final HR-PES measurements. No diffraction pattern was observed, however,
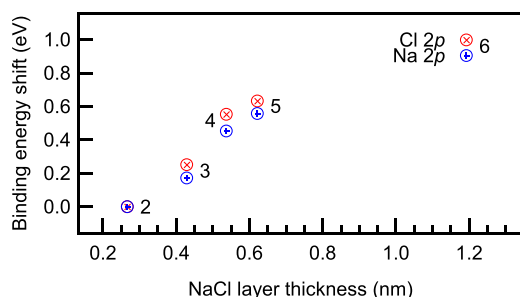
FIG. 5. The cumulative binding energy shift of the Cl 2*p* and Na 2*p* core levels as a function of deposited NaCl layer thickness. The spectrum number assigned to a pair of data points corresponds to the identification given in Figs. 1(c) and 1(d).

possibly due to electron irradiation induced damage or as a result of a wide distribution of crystallographic orientations of NaCl.

CONCLUSIONS

The interaction between NaCl and epitaxial silicene on $ZrB_2(0001)$ thin films was studied using synchrotron-based high-resolution photoelectron spectroscopy. The deposition of NaCl caused the appearance of Si 2*p* intensity overlapping with the expected binding energies of Si–Cl$_x$ (x = 1-3) species, as a result of dissociative chemisorption of NaCl. With increased NaCl deposition, the majority of epitaxial silicene reacted to form Si–Cl$_x$ species.

ACKNOWLEDGMENTS

[1] S. Cahangirov, M. Topsakal, E. Aktürk, H. Şahin, and S. Ciraci, Phys. Rev. Lett. **102**, 236804 (2009).

[2] C. C. Liu, W. Feng, and Y. Yao, Phys. Rev. Lett. **107**, 076802 (2011).

[3] P. Vogt, P. De Padova, C. Quaresima, J. Avila, E. Frantzeskakis, M. C. Asensio, A. Resta, B. Ealet, and G. Le Lay, Phys. Rev. Lett. **108**, 155501 (2012).

[4] L. Meng, Y. Wang, L. Zhang, S. Du, R. Wu, L. Li, Y. Zhang, G. Li, H. Zhou, W. A. Hofer, and H.-J. Gao, Nano Lett. **13**, 685 (2013).

[5] A. Fleurence, R. Friedlein, T. Ozaki, H. Kawai, Y. Wang, and Y. Yamada-Takamura, Phys. Rev. Lett. **108**, 245501 (2012).

[6] Y. Du, J. Zhuang, J. Wang, Z. Li, H. Liu, J. Zhao, X. Xu, H. Feng, L. Chen, K. Wu, X. Wang, and S. X. Dou, Sci. Adv. **2**, e1600067 (2016).

[7] P. De Padova, C. Ottaviani, C. Quaresima, B. Olivieri, P. Imperatori, E. Salomon, T. Angot, L. Quagliano, C. Romano, A. Vona, M. Muniz-Miranda, A. Generosi, B. Paci, and G. Le Lay, 2D Mater. **1**, 21003 (2014).

[8] A. Molle, C. Grazianetti, D. Chiappe, E. Cinquanta, E. Cianci, G. Tallarida, and M. Fanciulli, Adv. Funct. Mater. **23**, 4340 (2013).

[9] R. Friedlein, H. Van Bui, F. B. Wiggers, Y. Yamada-Takamura, A. Y. Kovalgin, and M. P. de Jong, J. Chem. Phys. **140**, 204705 (2014).

[10] D.-L. Sun, D.-Y. Wang, H.-F. Du, W. Ning, J.-H. Gao, Y.-P. Fang, X.-Q. Zhang, Y. Sun, Z.-H. Cheng, and J. Shen, Appl. Phys. Lett. **94**, 12504 (2009).

[11] R. T. Poole, J. G. Jenkin, J. Liesegang, and R. C. G. Leckey, Phys. Rev. B **11**, 5179 (1975).

[12] C. Raptis, Phys. Rev. B **33**, 1350 (1986).

[13] Y. Yamada-Takamura, F. Bussolotti, A. Fleurence, S. Bera, and R. Friedlein, Appl. Phys. Lett. **97**, 73109 (2010).

[14] R. Friedlein, A. Fleurence, K. Aoyagi, M. P. de Jong, H. Van Bui, F. B. Wiggers, S. Yoshimoto, T. Koitaya, S. Shimizu, H. Noritake, K. Mukai, J. Yoshinobu, and Y. Yamada-Takamura, J. Chem. Phys. **140**, 184704 (2014).

[15] V. Stolyarova, D. Sichen, and S. Seetharaman, Vacuum **46**, 871 (1995).

[16] K. Siegbahn, U. Gelius, H. Siegbahn, and E. Olson, Phys. Scr. **1**, 272 (1970).

[17] A. Fleurence and Y. Yamada-Takamura, Appl. Phys. Lett. **110**, 041601 (2017).

[18] S. Tanuma, C. J. Powell, and D. R. Penn, Surf. Interface Anal. **21**, 165 (1994).

[19] C.-C. Lee, J. Yoshinobu, K. Mukai, S. Yoshimoto, H. Ueda, R. Friedlein, A. Fleurence, Y. Yamada-Takamura, and T. Ozaki, Phys. Rev. B **95**, 115437 (2017).

[20] J.-Y. Chung, H.-D. Li, W.-H. Chang, T. C. Leung, and D.-S. Lin, Phys. Rev. B **83**, 085305 (2011).

[21] C.-Y. Chang, H.-D. Li, S.-F. Tsay, S.-H. Chang, and D.-S. Lin, J. Phys. Chem. C **116**, 11526 (2012).

[22] J. Matsuo, K. Karahashi, A. Sato, and S. Hijiya, Jpn. J. Appl. Phys. **31**, 2025 (1992).

[23] S. Rivillon, Y. J. Chabal, L. J. Webb, D. J. Michalak, N. S. Lewis, M. D. Halls, and K. Raghavachari, J. Vac. Sci. Technol. A **23**, 1100 (2005).

[24] Z. H. Lu, M. J. Graham, D. T. Jiang, and K. H. Tan, Appl. Phys. Lett. **63**, 2941 (1993).

[25] R. Bennewitz, V. Barwich, M. Bammerlin, C. Loppacher, M. Guggisberg, A. Baratoff, E. Meyer, and H.-J. Güntherodt, Surf. Sci. **438**, 289 (1999).